Chapter 4
Potential of Carbon Nanotubes for Cancer Cells Thermolysis in an RF Exposing Field

M.V. Shuba, S.A. Maksimenko, G.Ya. Slepyan, and G.W. Hanson

Abstract We study the effective dielectric permittivity and relative absorption rate for suspensions of singlewall carbon nanotubes (SWCNT) in the radiofrequency and microwave ranges. We show a strong influence of the carbon nanotube length and conductivity, as well as host media conductivity, on the energy absorption enhancement in SWCNT-based suspensions. The presented results show the possibility for realization of a high thermal contrast of the SWCNT-based agents for medical imaging and cancer cells thermolysis in the radiofrequency and microwave ranges.

Keywords Carbon nanotubes • Thermolysis • Absorption enhancement • Cancer cell • Radiofrequency

4.1 Introduction

Recent studies on the use of carbon nanotubes (CNTs) as thermal contrast agents for cancer cells thermal destruction in a radiofrequency field [1] as well as for the microwave detection and treatment of breast cancer [2, 3] have demonstrated a promising potential of CNT-enhanced low-frequency electromagnetic treatment of deep tissues. In this area, researchers face a set of biomedical and biochemical problems such as citotoxicity of CNTs, their solubility, selective embedding of

M.V. Shuba (✉) • S.A. Maksimenko • G.Ya. Slepyan
Institute for Nuclear Problem, Belarus State University,
11 Bobruiskaya str., 220030 Minsk, Belarus
e-mail: mikhail.shuba@gmail.com

G.W. Hanson
Department of Electrical Engineering, University of Wisconsin-Milwaukee,
3200 N. Cramer St., Milwaukee, WI 53211, USA

Y.N. Shunin and A.E. Kiv (eds.), *Nanodevices and Nanomaterials for Ecological Security*, NATO Science for Peace and Security Series B: Physics and Biophysics, DOI 10.1007/978-94-007-4119-5_4,

CNTs into malignant cells, their degradation and/or removal from tissues after treatment, etc. (see review articles [4] and Refs. [5–9] in addition to [1, 2]). Leaving biomedical aspects for a separate analysis, in the present paper we report the physical model of the radiofrequency field absorption by carbon nanotubes embedded in a conductive host, initially developed in [10–12]. We theoretically study the effective dielectric parameters of single-wall carbon nanotube (SWCNT) suspensions in the frequency range from 1 MHz to 60 GHz. For optimization of possible future experiments on the realization of high electromagnetic energy absorption enhancement, we investigate the influence of different parameters – frequency of incident radiation, SWCNT length and conductivity, and also host conductivity – on the SWCNT absorption enhancement in the conductive host, since the conductivity of the living cell components varies in a wide range. As an example [13], for liver cells the conductivity of cytoplasm is about 0.5 S/m while the conductivity of nuclear and mitochondrial material approaches 5 S/m. First measurements of the rf permittivity and electrical conductivity of biocompatible electrolyte SWCNT – based colloids has been reported in Ref. [14].

4.2 Theoretical Consideration

Let us consider the effective dielectric parameters of a SWCNT suspension in the microwave and radiofrequency ranges. For low volume fractions of SWCNT inclusions in a host medium we shall apply the Waterman-Truell formula adopted to estimate the relative permittivity of SWCNT suspensions [15],

$$\varepsilon_{eff}(\omega) = \varepsilon_w(\omega) + \frac{1}{3\varepsilon_0}\sum_j \int_0^\infty \alpha_j(\omega, L) N_j(L) dL, \tag{4.1}$$

where $\omega = 2\pi f$ and f are angular frequency and frequency of the electromagnetic field, respectively; ε_w is the complex relative permittivity of the host medium; $\varepsilon_0 = 8.85 \times 10^{-12}$ F/m; the function $N_j(L)$ describes the density number of SWCNTs of type j, length L, and radius R_j; the factor 1/3 in Eq. 4.1 is due to the random orientations of the SWCNTs; $\alpha_j(\omega, L)$ is the axial polarizability of an isolated SWCNTs of type j that can be calculated using the integral equation technique described in Ref. [11]. As it has been shown in Ref. [15], the axial polarizability of all metallic tubes depends slightly on the nanotube radius, therefore we do not take variations in radius into account and, instead, we model all metallic SWCNTs as being of a single type.

To evaluate the enhancement of electromagnetic energy absorption due to additional SWCNTs in the solution, we introduce a relative absorption rate

$$\theta = \frac{P_s}{P_h} = \frac{\mathrm{Im}[\varepsilon_{eff}]}{\mathrm{Im}[\varepsilon_h]} \tag{4.2}$$

where P_s and P_h are the powers dissipated in the SWCNT suspension and in a pure suspension without SWCNTs, respectively.

If the host is a lossy medium, then large intensity of the scattered field leads to large absorption in the host. In order to calculate dissipation of the scattered field in the host we introduce a cylindrical cell with the radius $R_{cell} \gg R$ and the length equal to the nanotube length L; the cell volume is $V_{cell} = \pi R_{cell}^2 L$. The SWCNT is located inside this cell on the cell axis. According to Ref. [2], we introduce a normalized absorption cross section Λ of a SWCNT in a lossy surrounding [11] when the external field is polarized to SWCNT axis,

$$\Lambda = \frac{P_w - P_{0w} + P_c}{I_0 S}, \tag{4.3}$$

where P_w is a power dissipated in the host medium of the cell; P_{0w} is the power dissipated in the cell without a SWCNT; P_c is a power dissipated in the SWCNT itself, $I_0 = 0.5|\sqrt{\varepsilon_w/\mu_0}||E_0|^2 \cos(\varphi)$ is the intensity of the incident field, $\varphi = \arg[\sqrt{\varepsilon_w}]$, E_0 is the amplitude of external field, and $S = 2\pi RL$ is the area of the SWCNT surface. The method for calculation of dissipated powers P_w, P_{0w} and P_{0w} is presented in Ref. [11]. For sufficiently large R_{cel} the value of Λ is almost independent of the cell volume.

4.3 Numerical Results

For illustrative results, we have considered three types of suspensions: (i) the suspension comprising only identical metallic zigzag (15,0) SWCNTs (*m*-suspension); (ii) the suspension comprising only identical semiconducting zigzag (14,0) SWCNTs (*s*-suspension); (iii) the suspension comprising the mixture of identical (14,0) SWCNTs and identical (15,0) SWCNTs (*ms*-suspension), where the ratio of the density of metallic SWCNTs (*m*-SWCNTs) to the density of semiconducting SWCNTs (*s*-SWCNTs) has been taken to be equal to 1/2. The volume fraction of all the considered SWCNT suspensions has been taken as 5.7×10^{-5}, that corresponds to 150 mg/L mass fraction of (15,0) SWCNTs for m-suspension.

Although we make calculations for a composite of zigzag SWCNTs, all the presented results are true for composites with SWCNTs of different chirality. This follows from the fact that the axial surface conductivity [Eq. (24) in Ref. [16]] and axial tube polarizability [Eq. (2) in Ref. [15]] are practically the same for all types of metallic SWCNTs, whether chiral or achiral, of identical radius and length. The conductivity of small radius (1–3 nm) semiconducting tubes in the microwave and radiofrequency ranges does not depend on the chirality, because it is determined mostly by the impurity of doping mechanisms in SWCNTs. Therefore, we shall describe the semiconducting SWCNTs with only one type – zigzag (14,0) SWCNTs with effective conductivity σ_s (see below).

In all calculations the conductivity σ_m of m-SWCNTs has been taken using the Drude-law [16] with electron relaxation time $\tau = 2 \times 10^{-14}$ s, which is close to the value $\tau = 3.3 \times 10^{-14}$ s obtained in Ref. [15]. As it has been shown in Ref. [11], the absorption parameters of m-SWCNTs in a conductive host do not change substantially with the increasing τ from 2×10^{-14} s to larger magnitudes. The value of s-SWCNT conductivity σ_s can be varied in a wide range with variations in the technological method of SWCNTs preparation and purification, because it strongly depends on SWCNT impurity doping. If not otherwise mentioned, we shall suppose $\sigma_s = 0.001\sigma_m$.

For example, at frequency 10 MHz the axial surface conductivity of metallic (15,0) and semiconducting (14,0) zigzag SWCNTs have been taken respectively as $\sigma_m = 1.46 \times 10^{-3} + i1.84 \times 10^{-9}$ S and $\sigma_s = 1.37 \times 10^{-6} + i1.72 \times 10^{-12}$ S.

We shall demonstrate our numerical results in the radio and microwave frequency range from 1 MHz to 60 GHz. In all calculations the dispersion law for the host permittivity is taken as for a saline solution according to the Cole-Cole relaxation function:

$$\varepsilon_w(\omega) = \varepsilon(\infty) + \frac{\varepsilon(0) - \varepsilon(\infty)}{1 - (i\omega\tau_w)^{1-\alpha}} + \frac{\sigma_w}{\omega\varepsilon_0}. \tag{4.4}$$

The parameters of Eq. 4.4 have been taken from the measurement data in Ref. [14] for saline solution: $\varepsilon(\infty) = 4.5$, $\alpha = 0.02$, $\varepsilon(0) = 76$, $\tau_w = 8.11 \times 10^{-12}$ s, σ_w is the host conductivity, which is supposed to be constant in the chosen frequency range.

The mechanisms of radiofrequency electromagnetic energy dissipation for both s-SWCNTs and m-SWCNTs embedded in a nonconductive and conductive host have been considered in Refs. [10] and [11], respectively. The theoretical model of the effective parameters of SWCNT-saline suspensions given in Ref. [12] describes precisely the experimental results of Ref. [14].

Figure 4.1 shows the space distribution of the intensity enhancement factor $\xi = |E|^2/|E_0|^2$ of a m-SWCNT with the length $L = 2$ μm (Fig. 4.1a) and $L = 0.2$ μm (Fig. 4.1b), when m-SWCNT is exposed to electromagnetic field at frequency 10 MHz and polarization vector to be along SWCNT axis; E and E_0 is the amplitude of the scattered and incident electric fields, respectively. The m-SWCNT is aligned parallel to the z axis of a cylindrical coordinate system (ρ, z, ϕ), whose origin ($z = 0$, $\rho = 0$) is collocated with the nanotube geometrical center. As the scattered field is symmetric in relation to the plane $z = 0$, only the right half of the m-SWCNT is shown in Fig. 4.1. Near the left half of the tube the distribution of ξ is the same.

Due to the edge effects a large surface density of electric charge concentrates near the SWCNT edges. This charge induces an electric field with a large radial component, resulting in strong field intensity enhancement outside the SWCNT. Thus, SWCNTs can concentrate electromagnetic energy near the SWCNT surface and, therefore, enhance power absorption in the conductive host. Let us note, that the field is concentrated stronger near the longer tubes (compare Fig. 4.1a and b).

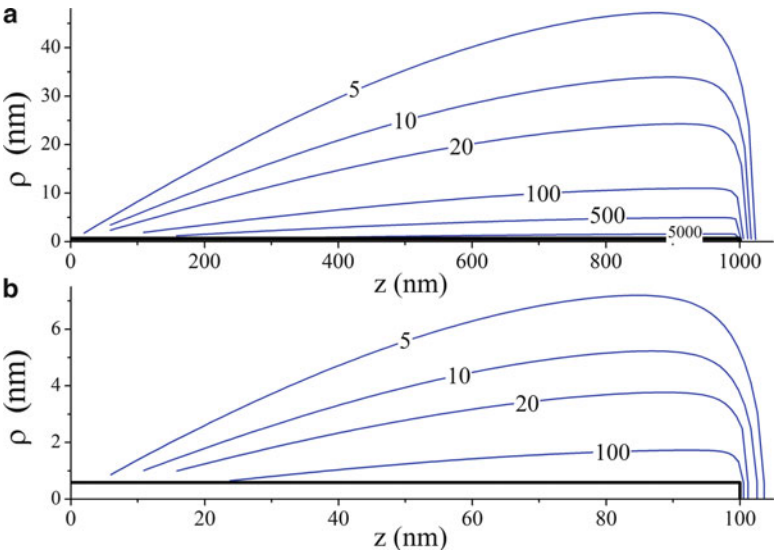

Fig. 4.1 The constant-value lines of the intensity enhancement factor $\xi(\rho, z)$ in the vicinity of the right half of metallic (15,0) zigzag SWCNTs with length $L = 2$ μm (**a**) and $L = 0.2$ μm (**b**). The right half of the SWCNT is shown by the *thick black line*. The relative dielectric constant of the host is $\varepsilon_w = 76 - 917i$ ($\sigma_w = 0.5$ S/m). The frequency is $f = 10$ MHz

As the conductivity of the components of a living cell vary in a wide range, we shall analyze the energy dissipation in SWCNT suspensions at different host conductivities σ_w. Figure 4.2 shows the dependence of the effective relative permittivity ε_{eff} on the host conductivity σ_w for different SWCNT suspensions. As shown in Fig. 4.2, at frequency 10 MHz the *m*-SWCNTs contribute strongly to the value of ε_{eff} in a wide range of host conductivity, whereas the contribution of *s*-SWCNT is strong only at a small value of σ_w.

We define a critical host conductivity as the conductivity of the host medium for which the real part of SWCNT polarizability $\mathrm{Re}[\alpha]$ is 10% smaller than $\mathrm{Re}[\alpha]$ at zero host conductivity, i.e., when $\mathrm{Re}[\alpha]|_{\sigma_w=\sigma_w^{(cr)}} = 0.9\mathrm{Re}[\alpha]|_{\sigma_w=0}$. So $\sigma_w^{(cr)} \approx 0.005$ S/m and $\sigma_w^{(cr)} \approx 2$ S/m for *s*- and *m*-suspension in Fig. 4.2, respectively. Generally, we can define two regions of the host conductivity, which are characterized by different behavior of the SWCNT polarizability. In the region of low host conductivity $\sigma_w < \sigma_w^{(cr)}$ we have $\mathrm{Re}[\varepsilon_{eff}]\big|_{\sigma_w<\sigma_w^{(cr)}} \approx \mathrm{Re}[\varepsilon_{eff}]\big|_{\sigma_w=0} > \mathrm{Re}[\varepsilon_w]$ that is explained by a slight influence of the host medium on the SWCNT polarizability. In the region of high host conductivity $\sigma_w > \sigma_w^{(cr)}$ the value $\mathrm{Re}[\varepsilon_{eff}]$ decreases with the value σ_w increasing. Such behavior of effective permittivity can be explained by the screening effect in a SWCNT embedded into the strongly conductive host. At high host conductivity the charge separation occurs not only in the SWCNT but also in the conductive host near the carbon nanotube surface, resulting in diminishing the effective field inside the carbon nanotube and, consequently, in diminishing the SWCNT polarizability. Let us note that (i) critical host conductivity $\sigma_w^{(cr)}$ for

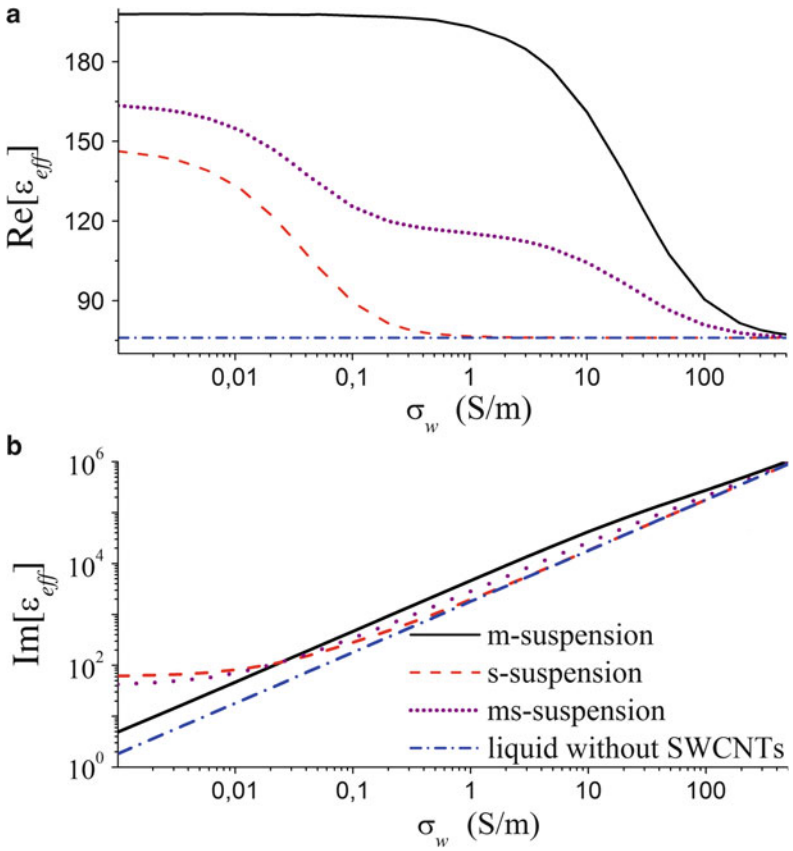

Fig. 4.2 The real (**a**) and imaginary (**b**) part of effective permittivity ε_{eff} of SWCNT suspension versus the host liquid conductivity σ_w. The calculation was made for *m*-suspension (*solid line*), *s*-suspension (*dashed line*), and *ms*-suspension (*dotted line*) at mass SWCNT fraction 150 mg/L and frequency 10 MHz. $L = 1$ μm. The *dash-dotted lines* correspond to the parameters of pure host media without SWCNTs

s-SWCNT is smaller than the value $\sigma_w^{(cr)}$ for *m*-SWCNT, i.e. the value $\sigma_w^{(cr)}$ increases with the increase of CNT conductivity; (ii) the value $\sigma_w^{(cr)}$ decreases with the increase of SWCNT length or the decrease of incident field frequency.

Figure 4.3 shows the relative absorption rate θ for different types of SWCNT-suspensions versus host media conductivity. As shown in Fig. 4.3, the rate of energy dissipation in the s-suspension (m-suspension) at 10 MHz and $\sigma_w = 0.01$ S m^{-1} is about 4.5 (2.6) times larger than for host liquid without SWCNTs. Thus, at small values of surrounding conductivity σ_w the energy dissipation is stronger for suspensions with semiconducting SWCNTs than for suspensions with metallic SWCNTs. The same tendency is illustrated in Ref. [1] for the case of a non-conductive host.

Figure 4.4 shows the frequency dependence of the real (Fig. 4.4a) and imaginary (Fig. 4.4b) parts of effective relative permittivity ε_{eff} for different types of

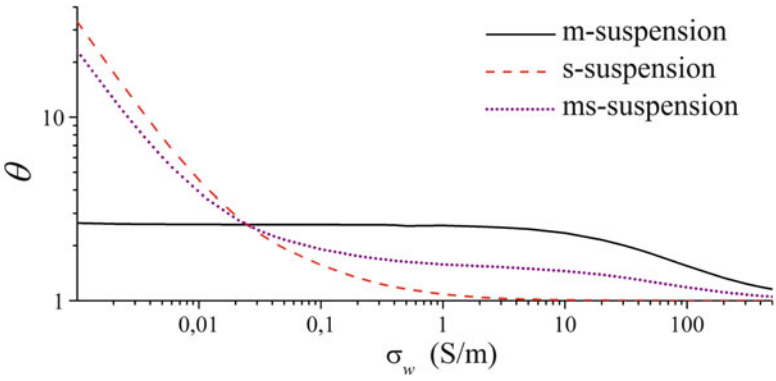

Fig. 4.3 The relative absorption rate θ for *m*-suspension (*solid line*), *s*-suspension (*dashed line*) and *ms*-suspension (*dotted line*) versus the conductivity σ_w of host media at frequency 10 MHz and mass SWCNTs fraction 150 mg/L. Carbon nanotube length is $L = 1$ μm

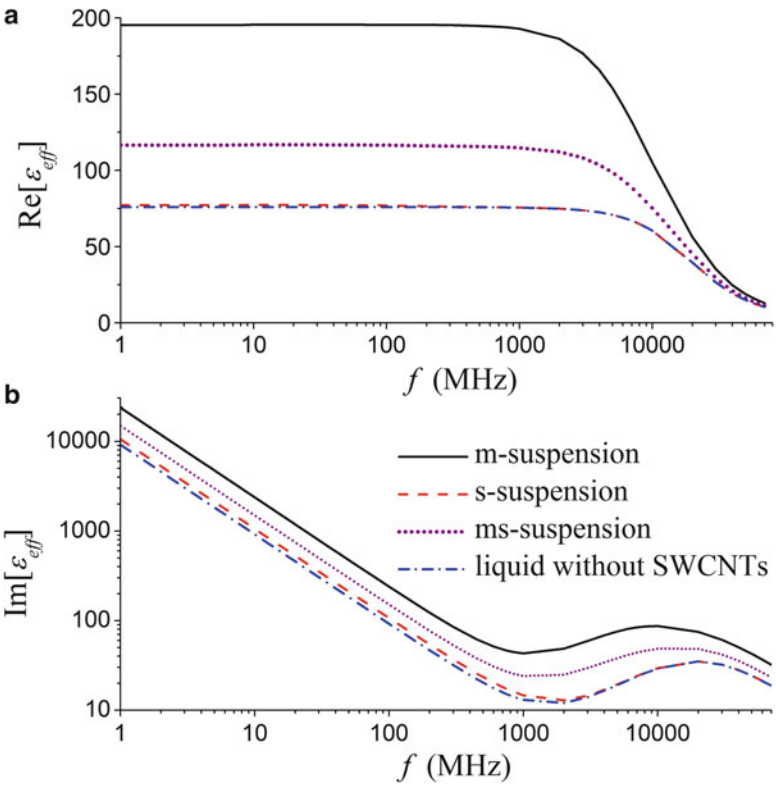

Fig. 4.4 Frequency dependence of the real (**a**) and imaginary (**b**) parts of effective relative permittivity ε_{eff} for *m*-suspension (*solid line*), *s*-suspension (*dashed line*) and *ms*-suspension (*dotted line*) and pure host media without SWCNT (*dash-dotted line*) at mass SWCNT fraction 150 mg/L and host conductivity $\sigma_w = 0.5$ S/m. The length of SWCNTs is $L = 1$ μm

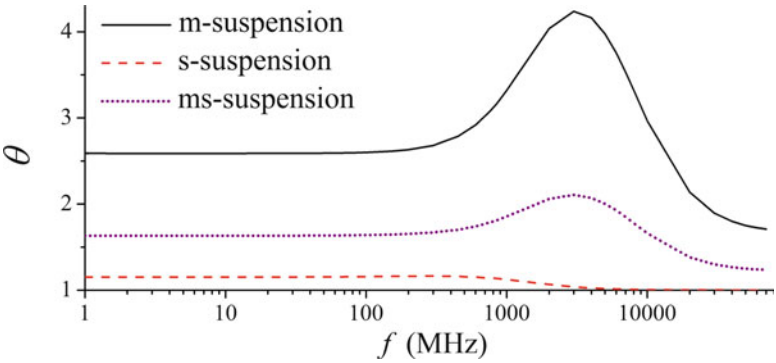

Fig. 4.5 Frequency dependence of the relative absorption rate θ for *m*-suspension (*solid line*), *s*-suspension (*dashed line*) and *ms*-suspension (*dotted line*) at the host conductivity $\sigma_w = 0.5$ S/m and SWCNTs mass fraction 150 mg/L. The length of SWCNTs is $L = 1$ μm

SWCNT-suspensions at host conductivity $\sigma_w = 0.5$ S/m. As shown in Fig. 4.4, the contribution of *m*-SWCNTs (*s*-SWCNTs) to effective permittivity is large (small) in the considered frequency range. Here we define a critical frequency f_{cr} as the frequency, which divides two electromagnetic regimes and can be found from the expression for SWCNT polarizability $\mathrm{Re}[\alpha]\big|_{f=f_{cr}} = 0.9\mathrm{Re}[\alpha]\big|_{f=0}$. For m-suspension in Fig. 4.4 we have $f_{cr} = 2$ GHz.

In the range of $f<f_{cr}$ $\mathrm{Re}[\varepsilon_{eff}]\big|_{f<f_{cr}} \approx \mathrm{Re}[\varepsilon_{eff}]\big|_{f=0} > \mathrm{Re}[\varepsilon_w]$, that corresponds to quasistatic regime – the real part of *m*-SWCNT polarizability is the same as in electrostatic case at $f \to 0$. In the range of $f>f_{cr}$ – dynamical regime – the value $\mathrm{Re}[\varepsilon_{eff}]$ decreases with the frequency increase. Let us note that the value f_{cr} increases with the CNT length L decrease or SWCNT conductivity increase. In the dynamical regime at $f>f_{cr}$ the effect of near field enhancement in SWCNT and the screening effect in SWCNT bundles and MWCNT (see Ref. [11]) become less significant, i.e. the electromagnetic field penetrates deeper inside the SWCNT-bundle and MWCNT, resulting in the increase of electromagnetic absorption cross-section of these particles.

Figure 4.5 shows the frequency dependence of relative absorption rate θ on different types of SWCNT suspensions. As shown in Fig. 4.5, the value θ for *m*- and *ms*-suspensions is constant in a wide frequency range $f<1$ GHz. At frequency 4 GHz the value θ has a wide peak, which occurs due to the inhomogeneous host medium frequency dispersion. At frequencies higher than 4 GHz the value θ decreases due to being in the dynamical regime, which is accompanied by a decrease of the near-field enhancement in metallic SWCNTs.

Figure 4.6 shows the real (Fig. 4.6a, d) and imaginary (Fig. 4.6b, e) parts of the effective relative permittivity ε_{eff} and the absorption coefficient γ (Fig. 4.6c, f) for different types of SWCNT suspensions at different frequencies. As shown in Fig. 4.6, the values $\mathrm{Im}[\varepsilon_{eff}]$ and γ increase with the SWCNT length increase both at 10 MHz and 1 GHz. The value $\mathrm{Re}[\varepsilon_{eff}]$ has a non-monotonic dependence on L with the maximum, which occurs at critical length L_{cr} (at $f = 1$ GHz, $L_{cr} = 0.6$ μm and $L_{cr} = 4$ μm for s-suspension and m-suspension, respectively).

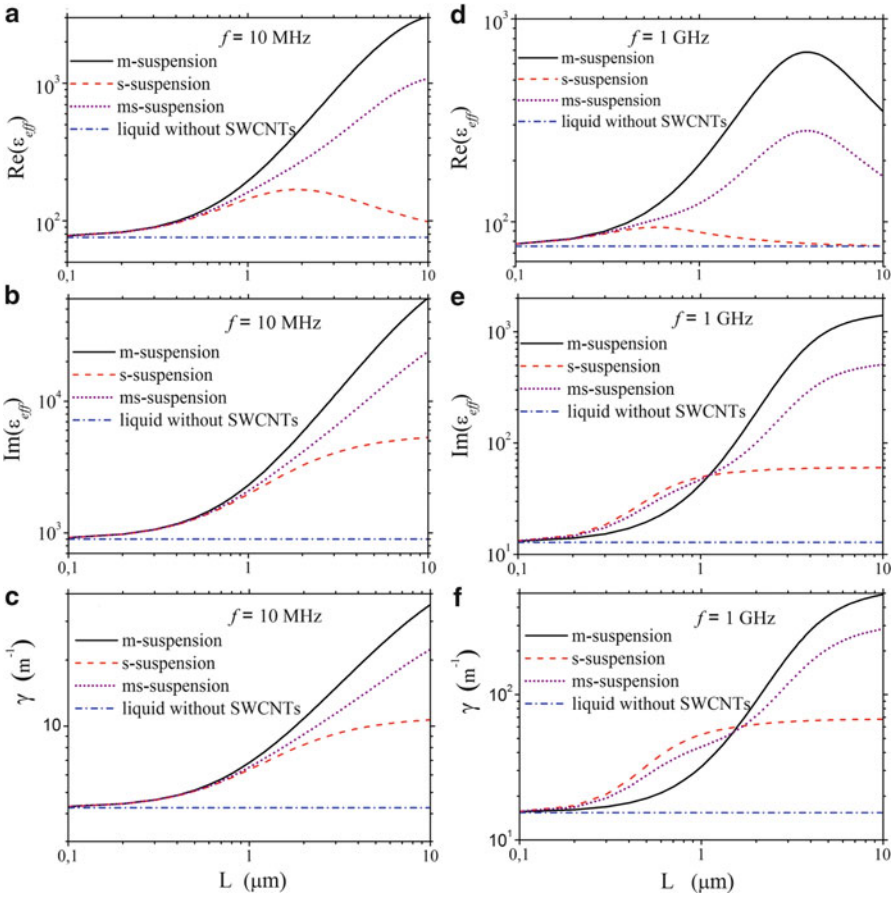

Fig. 4.6 The real (**a**, **d**) and imaginary (**b**, **e**) part of effective relative permittivity ε_{eff} and absorption coefficient (**c**, **f**) [$\gamma = 2\pi f \mathrm{Im}[(\varepsilon_{eff})^{1/2}]/c$, c is light velocity in vacuum] for *m*-suspension (*solid line*), *s*-suspension (*dashed line*) and *ms*-suspension (*dotted line*) and pure host liquid without SWCNT (*dash-dotted line*) versus nanotube length L, at mass SWCNT fraction 150 mg/L, host conductivity $\sigma_w = 0.5$ S/m and frequencies $f = 10$ MHz (**a**, **b**, **c**) and 1 GHz (**d**, **e**, **f**). The conductivity of *s*-SWCNT σ_s satisfies the ratio $\sigma_s = 0.03\sigma_m$, where σ_m is the conductivity of *m*-SWCNT of the same radius at relaxation time $\tau = 2 \times 10^{-14}$ s

The value L_{cr} is the characteristic length, which defines the boundary of two different regimes of SWCNT interactions with electromagnetic radiation: (i) at $L<L_{cr}$ the depolarizing field in SWCNT is strong due to the finite length effects (ii) at $L>L_{cr}$ the influence of SWCNT edges is sufficiently small and the effective field (which induces current on the SWCNT) is close to the incident field. The value L_{cr} increases (i) with the frequency decreasing and (ii) with SWCNT conductivity increase or (iii) with the host conductivity decrease. Therefore the value L_{cr} for m-suspension is larger than the value L_{cr} for s-suspension.

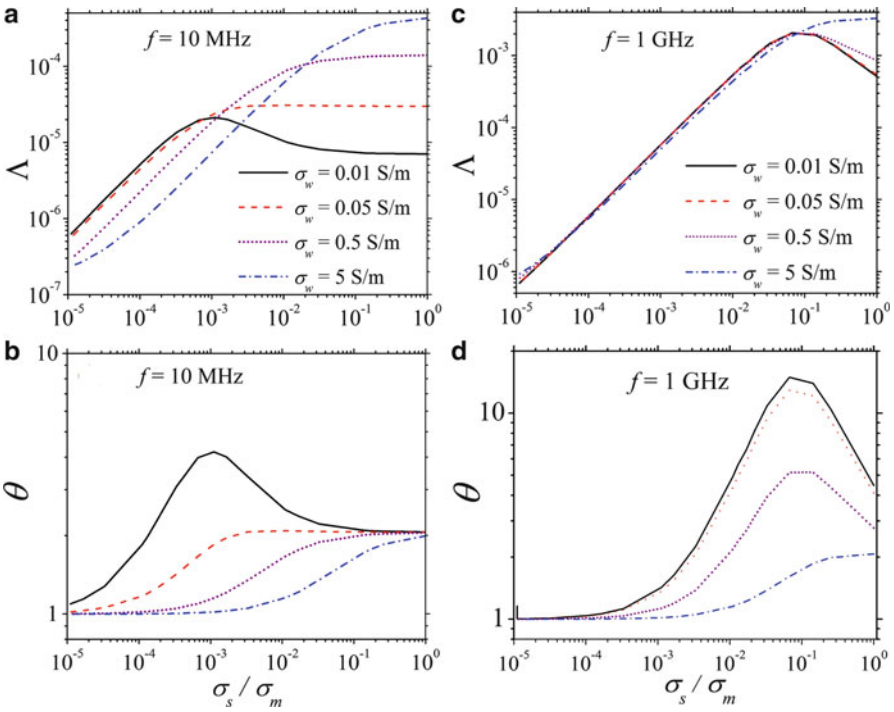

Fig. 4.7 Normalized absorption cross section Λ for *s*-SWCNT (**a**, **c**) and relative absorption rate (**b**, **d**) for *s*-suspension versus SWCNT conductivity σ_s at different host conductivity $\sigma_w = 0.01$ S/m (*solid line*), $\sigma_w = 0.05$ S/m (*dashed line*), $\sigma_w = 0.5$ S/m (*dotted line*), $\sigma_w = 5$ S/m (*dash-dotted line*). The length of *s*-SWCNT is $L = 1$ μm. The value σ_s is normalized on the conductivity σ_m of metallic SWCNT of the same radius: $\sigma_m = 1.72 \times 10^{-3} + i2.16 \times 10^{-9}$ S at 10 MHz and $\sigma_m = 1.72 \times 10^{-3} + i2.16 \times 10^{-7}$ S at 1 GHz

Let us also note that according to Fig. 4.6e, f, at frequency 1 GHz and nanotube length $L = 0.1$–1 μm the *s*-suspension absorbs better than *m*-suspension. Absorption cross-section of *s*-SWCNTs strongly depends on their conductivity σ_s and for non-conductive host at $\sigma_s = \sigma_s^{(\max)}$ the value of Λ has the maximal value [10].

Figure 4.7 shows the normalized absorption cross section Λ for *s*-SWCNT (Fig. 4.7a, c) and relative absorption rate θ (Fig. 4.7b, d) for *s*-suspension versus nanotube conductivity σ_s at different ranges of host conductivity and different frequencies. As shown in Fig. 4.7a, c, the value of $\sigma_{\max}$depends on frequency: $\sigma_s^{(\max)} = 0.001\sigma_m$ at $f = 10$ MHz and $\sigma_s^{(\max)} = 0.08\sigma_m$ at $f = 1$ GHz; here σ_m is defined in the caption of Fig. 4.7. The value $\sigma_s^{(\max)}$ increases with frequency f increasing and SWCNT length L decreasing. Moreover, at high host conductivity the maximum in the dependences of $\Lambda(\sigma_s)$ and $\theta(\sigma_s)$ is absent (see Fig. 4.7).

4.4 Conclusions

We have analyzed the effective parameters of SWCNT-based suspensions. We have shown that a small amount of SWCNTs (volume fraction of 5.7×10^{-5}) can enhance radiofrequency energy absorption more than 200% even in high conductive liquids. We show a strong dependence of absorption enhancement factor on the nanotube conductivity, nanotube length, host media conductivity and frequency range. The presented results show the possibility of realizing high thermal contrast, SWCNT-based agents for medical imaging technologies and cancer cells thermolysis in radiofrequency and microwave ranges.

Acknowledgements This research has been partially supported by the BRFFR under Projects No. F10R-002 and No. F10CO-020, EU FP7 under Projects No. FP7-230778 TERACAN, No. FP7-247007 CACOMEL, and No. FP7-266529 BY-NanoERA, and ISTC under Project No. B-1708.

References

1. Gannon CJ, Cherukuri P, Yakobson BI, Cognet L, Kanzius JS, Kittrell C, Weisman RB, Pasquali M, Schmidt HK, Smalley RE, Curley SA (2007) Carbon nanotube-enhanced thermal destruction of cancer cells in a noninvasive radiofrequency field. Cancer 110:2654–2665
2. Mashal A, Sitharaman B, Li X, Avti PK, Sahakian AV, Booske JH, Hagness SC (2010) Toward carbon-nanotube-based theranostic agents for microwave detection and treatment of breast cancer: enhanced dielectric and heating response of tissue-mimicking materials. IEEE Trans Biomed Eng 57:1831–1834
3. Shea JD, Kosmas P, Veen BDV, Hagness SC (2010) Contrast-enhanced microwave imaging of breast tumors: a computational study using 3D realistic numerical phantoms. Inverse Probl 26:074009
4. Gilstrap K, Hu X, Lu X, He X (2011) Nanotechnology for energy-based cancer therapies. Am J Cancer Res 1:507–519
5. Kam NWS, O'Connell MJ, Wisdom JA, Dai H (2005) Carbon nanotubes as multifunctional biological transporters and near-infrared agents for selective cancer cell destruction. Proc Natl Acad Sci USA 102:11600–11605
6. Shim M, Wong N, Kam S, Chen RJ, Li Y, Dai H (2002) Functionalization of carbon nanotubes for biocompatibility and biomolecular recognition. Nano Lett 2:285–288
7. Bellucci S, Chiaretti M, Cucina A, Carr GA, Chiaretti AI (2009) MWCNT buckypaper: toxicology and biological effects in vivo and in vitro. Nanomedicine 4:531–540
8. Zhou F, Xing D, Ou Z, Wu B, Resasco DE, Chen WR (2009) Cancer photothermal therapy in the near-infrared region by using single-walled carbon nanotubes. J Biomed Opt 142:021009
9. Kagan VE, Konduru NV, Feng W, Allen BL, Conroy J, Volkov Y, Vlasova II, Belikova NA, Yanamala N, Kapralov A, Tyurina YY, Shi J, Kisin ER, Murray AR, Franks J, Stolz D, Gou P, Klein-Seetharaman J, Fadeel B, Star A, Shvedova A (2010) Carbon nanotubes degraded by neutrophil myeloperoxidase induce less pulmonary inflammation. Nat Nanotechnol 5:354–359
10. Hanson GW, Patch SK (2009) Optimum electromagnetic heating of nanoparticle thermal contrast agents at rf frequencies. J Appl Phys 106:054309
11. Shuba MV, Slepyan GYa, Maksimenko SA, Hanson GW (2010) Radiofrequency field absorption by carbon nanotubes embedded in a conductive host. J Appl Phys 108:114302

12. Shuba MV, Slepyan GY, Maksimenko SA, Hanson GW (2011) RF and microwave electrical response of carbon nanotube saline solutions for potential biomedical applications. Nanosci Nanotechnol Lett 3:885–888
13. Raicu V, Saibara T, Enzan H, Irimajiri A (1998) Dielectric properties of rat liver in vivo: analysis by modeling hepatocytes in the tissue architecture. Bioelectrochem Bioenerg 47:333–342
14. Gach HM, Nair T (2010) Radiofrequency interaction with conductive colloids: permittivity and electrical conductivity of single-wall carbon nanotubes in saline. Bioelectromagnetics 31:582
15. Slepyan GYa, Shuba MV, Maksimenko SA, Thomsen C, Lakhtakia A (2010) Terahertz conductivity peak in composite materials containing carbon nanotubes: theory and interpretation of experiment. Phys Rev B 81:205423
16. Slepyan GY, Maksimenko SA, Lakhtakia A, Yevtushenko O, Gusakov AV (1999) Electrodynamics of carbon nanotubes: dynamic conductivity, impedance boundary conditions, and surface wave propagation. Phys Rev B 60:17136–17149